Energy & Environmental Science

PAPER

View Article Online
View Journal | View Issue

Cite this: *Energy Environ. Sci.*, 2017, **10**, 1207

Identifying and suppressing interfacial recombination to achieve high open-circuit voltage in perovskite solar cells†

Juan-Pablo Correa-Baena, ‡*[a] Wolfgang Tress,*[b] Konrad Domanski,[b] Elham Halvani Anaraki, [ac] Silver-Hamill Turren-Cruz, [af] Bart Roose,[d] Pablo P. Boix,[e] Michael Grätzel,[b] Michael Saliba, [b] Antonio Abate [d] and Anders Hagfeldt [a]

Received 13th February 2017,
Accepted 24th March 2017

DOI: 10.1039/c7ee00421d

rsc.li/ees

With close to 100% internal quantum efficiency over the absorption spectrum, photocurrents in perovskite solar cells (PSCs) are at their practical limits. It is therefore imperative to improve open-circuit voltages (V_{OC}) in order to go beyond the current 100 mV loss-in-potential. Identifying and suppressing recombination bottlenecks in the device stack will ultimately drive the voltages up. In this work, we investigate in depth the recombination at the different interfaces in a PSC, including the charge selective contacts and the effect of grain boundaries. We find that the density of grain boundaries and the use of tunneling layers in a highly efficient PSC do not modify the recombination dynamics at 1 sun illumination. Instead, the recombination is strongly dominated by the dopants in the hole transporting material (HTM), spiro-OMeTAD and PTAA. The reduction of doping concentrations for spiro-OMeTAD yielded V_{OC}'s as high as 1.23 V in contrast to PTAA, which systematically showed slightly lower voltages. This work shows that a further suppression of non-radiative recombination is possible for an all-low-temperature PSC, to yield a very low loss-in-potential similar to GaAs, and thus paving the way towards higher than 22% efficiencies.

Broader context

Perovskite-based solar cells have emerged as a promising technology for highly efficient and low-cost photovoltaics. The high efficiencies so far reported go beyond 20% and have started to approach their practical limitations. Hence, efforts need to be made to improve recombination dynamics in order to push forward the V_{OC}. In this work, we investigate the interfacial recombination and show that for optimized systems the electron selective layer (*i.e.* SnO_2 in a planar perovskite solar cell furnishing over 20% power conversion efficiency) is not limiting the V_{OC}. Similarly, no change in the V_{OC} is detected when modifying the grain size from <100 to ~400 nm, suggesting no change in the recombination with an increase in grain boundaries. We then conclude that dopants in the organic hole transport layer limit the V_{OC}. Modifying dopant concentration can significantly boost the V_{OC} to achieve values of up to 1.23 V. This study sheds light on the importance that the hole transport layer has on the recombination dynamics and suggests further work to improve hole conductors that do not rely on dopants (*i.e.* metal oxides).

[a] *Laboratory of Photomolecular Science, Institute of Chemical Sciences and Engineering, École Polytechnique Fédérale de Lausanne, CH-1015-Lausanne, Switzerland. E-mail: jpcorrea@mit.edu*
[b] *Laboratory for Photonics and Interfaces, Institute of Chemical Sciences and Engineering, École Polytechnique Fédérale de Lausanne, CH-1015-Lausanne, Switzerland. E-mail: wolfgang.tress@epfl.ch*
[c] *Department of Materials Engineering, Isfahan University of Technology, Isfahan, 84156-83111, Iran*
[d] *Adolphe Merkle Institute, Chemin des Verdiers 4, CH-1700 Fribourg, Switzerland*
[e] *Energy Research Institute at Nanyang Technological University (ERI@N), 50 Nanyang Drive, Singapore 637553, Singapore*
[f] *Benemérita Universidad Autónoma de Puebla, Puebla, 7200, Mexico*

† Electronic supplementary information (ESI) available. See DOI: 10.1039/c7ee00421d

‡ Current address: Massachusetts Institute of Technology, Cambridge, MA, 02139, USA.

Introduction

Perovskite solar cells (PSCs) composed of organic-metal-halide structures have made impressive progress in just a few years with power conversion efficiencies (PCEs) jumping from 3.8%[1] in 2009 to a certified 22.1%[2] in 2016.[3] The general formula of the commonly used perovskite is ABX_3 containing an organic cation A, such as methylammonium (MA) or formamidinium (FA),[1,4] a divalent metal B, such as Pb or Sn,[5] and a halide X, such as bromine or iodine. The impressive performance achieved to date has been attributed to the exceptional material properties such as high defect tolerance[6] along with low charge recombination, high light absorption over the visible spectrum including

a sharp absorption onset and charge carrier diffusion lengths in the micrometre range.[7–10] In addition, PSC modules have potential for rapid energy payback, which is essential for large-scale application as a solar energy harvester.[11]

Currently, only a few reports exist with efficiencies above 20% and high open-circuit voltages (V_{OC}). All, except for that reported by Anaraki *et al.*,[12] use mesoporous layers.[13–15] The use of a simplified, low-temperature planar structure avoids the effects of the mesoporous infiltrated perovskite which has a different morphology to the capping layer of dense large grains. All the high voltage and efficiency PSCs have been prepared with mixed Pb-based perovskites, composed of MA, FA, Br and I. More recently, we have demonstrated that the addition of cesium (Cs) and rubidium (Rb) as monovalent cations helps suppress the detrimental yellow phase in the MA/FA mixed perovskite, yielding more reproducible PCEs close to 22%.[16,17]

In our earlier study,[18] using a SnO_2-based planar configuration (FTO/SnO_2/perovskite/spiro-OMeTAD/gold), we have shown a high V_{OC} of 1.19 V, for a 1.6 eV bandgap PSC. More recently we reported on a V_{OC} of 1.20 V by way of organic cation stoichiometry modification[19] and of 1.24 V by Rb incorporation, which further suppressed phase defects in the perovskite material. With photocurrents at their practical limits of 24 mA cm^{-2} (1.6 eV bandgap),[20,21] we can only make further efficiency gains by improving the V_{OC} and in turn the fill factor. Therefore, in order to go beyond these voltages, it is important to understand the recombination mechanisms in these devices to formulate a strategy approaching the thermodynamic limit, which is calculated to be 1.32 V for our perovskites with a bandgap of about 1.6 eV.[9]

In this work, we investigate in depth the recombination mechanisms at the different interfaces in a PSC, including the charge selective contacts and the effect of grain boundaries in the perovskite. By employing simple SnO_2 planar devices with efficiencies above 20% and V_{OC}'s of up to 1.23 V, we investigate the device layers that induce non-radiative recombination. We find that the recombination dynamics are strongly dominated by the dopant concentration in the hole selective layer (HSL) spiro-OMeTAD. Spiro-OMeTAD without Li-TFSI yields a high V_{OC} of 1.22 V decreasing monotonically as the dopant concentration increases. Low dopant concentrations also yield low fill factors (FF), suggesting a low conductivity in the HSL, and thus affecting the power conversion efficiency of the devices. This issue was overcome by exposing the doped-HSL devices to a nitrogen atmosphere, which boosted the V_{OC} without compromising much on FFs. This effect is believed to be due to the dedoping of the HSL by oxygen desorption, which reduces recombination centers, detrimental to a high V_{OC}.

Results

Fig. 1a shows a schematic of a device composed of fluorine-doped tin oxide (FTO), a 15 nm-thin, conformal SnO_2 by atomic layer deposition (ALD), a *ca.* 500 nm mixed ion perovskite layer, topped by a hole selective layer (either 30 nm PTAA or 200 nm spiro-OMeTAD) and an 80 nm gold electrode. The cross-sectional scanning electron micrograph (SEM) in Fig. 1b shows the relative flatness of the interfaces which makes it easy to study each component of the solar cell stack. Such devices reach an efficiency of >20% as shown by a representative current–voltage (*JV*) curve in Fig. 1c. The V_{OC} close to 1.2 V is remarkably high, but still more than 100 mV away from its thermodynamic limit, indicative of a considerable amount of non-radiative recombination. To identify its source, we vary the interfaces to the charge transport layers and the perovskite morphology and investigate the effects on V_{OC}.

One possible source of the interfacial recombination is the SnO_2 electron contact which might not be perfectly selective or defect free. To check whether considerable recombination occurs at the perovskite/SnO_2 interface, a thin, conformal Ga_2O_3 interlayer is introduced by atomic layer deposition. This widegap material has been shown to passivate surfaces of crystalline silicon solar cells.[23] Due to the high conduction and low valence band edges, Ga_2O_3 is supposed to block both electrons and holes (Fig. 2a). However, a sufficiently thin layer can allow for tunneling of an electron in the conduction band from the perovskite to the SnO_2 as indicated by the horizontal arrow in the sketch, while suppressing the interfacial recombination. The *JV* curves in Fig. 2b indeed show that the solar cells with thin (<1 nm) Ga_2O_3 interlayers work well. The fill factor is slightly reduced as

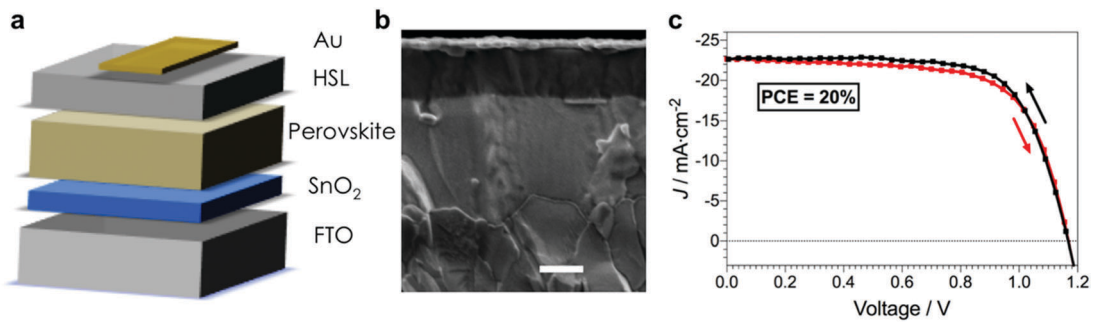

Fig. 1 Device configuration and a representative current–voltage curve. (a) Schematic of a typical device configuration. (b) A cross-sectional scanning electron microscopy image of a planar SnO_2 PSC (scale bar is 200 nm) and (c) current–voltage characteristics for a typical planar PSC with reverse and forward sweeps (10 mV s^{-1}), measured with a 0.16 cm^2 mask (0.25 cm^2 electrode area) at 1 sun illumination (AM 1.5G). The V_{OC} is 1.17 V, the current density is 23 mA cm^{-2} and the fill factor is 71% (68% for the forward scan) and the stabilized efficiency reaches 20%.

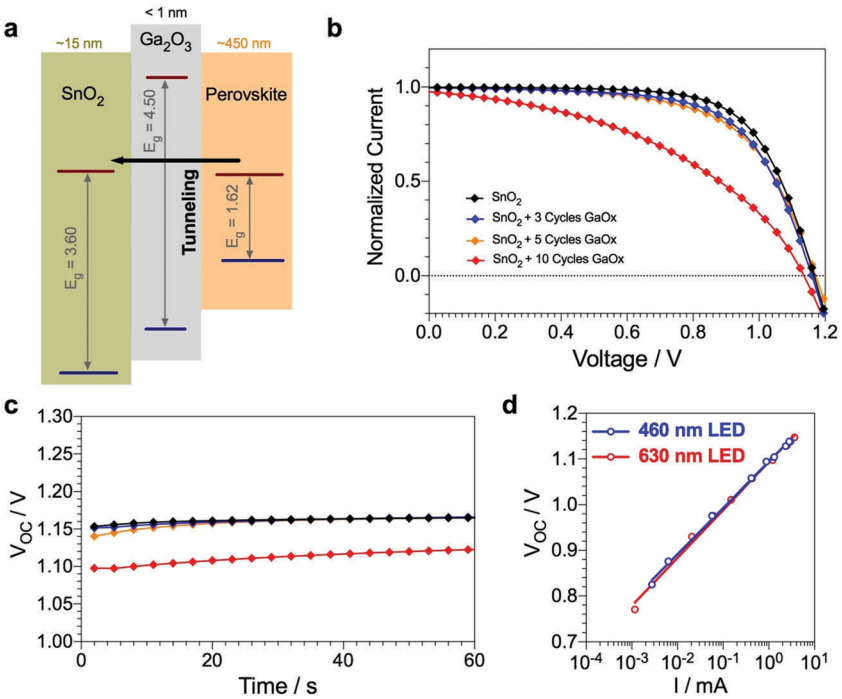

Fig. 2 Effect of tunneling layer (Ga_2O_3) thickness on the photovoltaic parameters of PSCs. (a) Schematic of the energetics of the SnO_2 electron selective layer[18] followed by sub-nanometer layers of Ga_2O_3 as tunneling layers,[22] and the perovskite absorber.[18] (b) Current–voltage characteristics normalized at J_{SC} (backward scan, 10 mV s^{-1}) and (c) V_{OC} evolution over time of devices with different Ga_2O_3 layer thicknesses (10 cycles = 1 nm). (d) V_{OC} as a function of the short-circuit current, which is proportional to light intensity, for a planar device illuminated with blue and red light.

expected from a highly resistive interlayer. Once the layer gets too thick (1 nm), the fill factor suffers from the hindered electron extraction through the Ga_2O_3, and the *JV* curves show the features of a solar cell with increased series resistance.

Interestingly, the V_{OC} is not affected by the Ga_2O_3 layer, indicating that the V_{OC} is not limited by the recombination at the SnO_2/perovskite interface. For the 1-nm-thick Ga_2O_3, the V_{OC} decreases, possibly due to the enhanced recombination in the perovskite or the interface with the spiro-OMeTAD, when the electrons are not extracted efficiently and the electric field peaks in the Ga_2O_3 layer.

In order to shed light on the role of the SnO_2 layer in the recombination dynamics, we investigated the V_{OC} as a function of illumination intensity, represented by the short-circuit current and shown in Fig. 2d. Exploiting the strong absorption of the perovskite material for high energy photons, the devices were tested using blue (460 nm) and red (630 nm) LEDs. The use of two wavelengths allows for the identification of recombination close to the ESL (when illuminated from the glass/FTO/ESL side and surface recombination is comparably faster than charge carrier redistribution) as more charge carriers are generated within the first 150 nm for blue light, compared to red light (Fig. S1, ESI†). Lower V_{OC} values for blue illumination, when compared to red illumination would mean that this interface is limiting the V_{OC}.[15,24] However, for our planar devices no V_{OC} difference is observed for blue and red illumination and the slope of the fitted line is around 110 mV $decade^{-1}$, indicating that the ESL is not the dominant limiting factor. This finding is consistent with the conclusion from the above investigation of Ga_2O_3 interlayers.

Grain boundaries are known to be a source of recombination in photovoltaic materials. That is why they are also suspected to be detrimental to the V_{OC} in PSCs,[15,25–27] although contrary results have been reported in the literature.[21,28–32] To tune the density of grain boundaries, PSCs are prepared using precursor solutions with different concentrations, yielding grains with average sizes ranging from <100 nm to ~400 nm, as deduced from the SEM top views in Fig. 3a–c (Fig. S2 for a full range, ESI†). Concomitantly, the thickness of the layer changed from roughly 80 nm to 400 nm (Fig. S3 shows the cross-sectional SEM images, ESI†). The *JV* curves normalized at the short circuit are shown in Fig. 3d. As we have reported earlier for mesoporous-TiO_2 based PSCs,[21] the fill factor decreases for films with a smaller grain size, pointing to inhibited charge transport from grain to grain. However, the V_{OC} does not show any systematic trend, and variations can be attributed to the variability from device to device. This is confirmed by the stabilized V_{OC} *vs.* time plotted in Fig. 3e, where the V_{OC} is between 1.18 and 1.20 V for all devices, with the smallest grains exhibiting the higher V_{OC}. To further confirm that the recombination under charge carrier densities relevant for solar operation is unaffected by grain boundaries, the external electroluminescence yield EQE_{EL} is detected during a voltage sweep and plotted as a function of the injection current in Fig. 3f. The EQE_{EL} quantifies the ratio between radiative and total (including non-radiative) recombination. It shows a slight hysteresis, and increases with the injection current as expected for a diode limited by Shockley–Read–Hall recombination.[33] Once the currents are in the order of the short circuit current under solar illumination, all curves

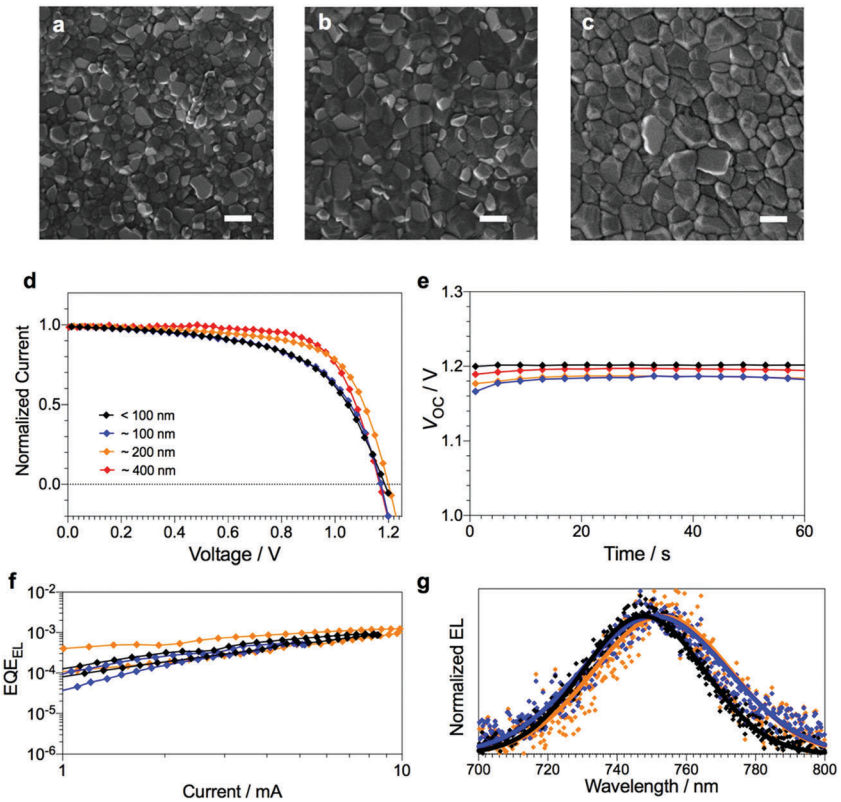

Fig. 3 Relationship between grain boundaries and photovoltaic parameters. Scanning electron microscopy of samples with grain sizes of (a) <100 nm (b) ~200 nm and (c) ~400 nm. (d) Current–voltage curves (backward scan, 10 mV s^{-1}) of PSCs with different perovskite grain dimensions and (e) V_{OC} *vs.* time of the same devices. (f) External quantum efficiency of electroluminescence (EQE_{EL}) as a function of current and (g) the respective spectra.

coincide, proving that non-radiative recombination rates are independent of this grain size variation. As bandgaps dependent on the crystal/grain size have been reported for these perovskite materials,[34] we investigate the bandgap using the EL spectra, which do not shift significantly, as shown in Fig. 3g. Therefore, for a highly efficient PSC, the density of grain boundaries in the investigated range does not modify significantly the recombination rate under solar illumination.

So far recombination at the ESL/perovskite interface and due to grain boundaries (small *vs.* large grains) could not be manipulated nor identified as a major bottleneck for V_{OC} in this device configuration at 1 sun illumination. Therefore, this prompted the study of the role of the HSL in recombination dynamics in PSCs. PTAA and spiro-OMeTAD were employed as the HSL in all the PSCs with record efficiencies, as they are capable of yielding efficiencies above 20% and record high voltages, and are therefore ideal to study recombination. It is important to note that PTAA and spiro-OMeTAD exhibit relatively similar current–voltage characteristics, with one exception being V_{OC}. Importantly, the difference between these two materials that serve as HSLs highlights the importance that this layer has on V_{OC}. On the other hand, when using different ESLs, be it mesoporous TiO_2,[16,21] or planar SnO_2,[12] no significant difference in V_{OC} (yielding above 1.2 V) has been shown.

We used intensity modulated photovoltage spectroscopy (IMVS) to estimate the recombination lifetime at the SnO_2 and the spiro-OMeTAD interfaces.[35,36] Fig. 4a displays a significantly slower recombination lifetime at the same open circuit voltage when the perovskite film is illuminated with blue light (460 nm) from the SnO_2 compared to the spiro-OMeTAD side (employing semitransparent electrodes). As the charge density is higher at the interface under illumination, the extracted lifetimes provide direct information about the recombination taking place at the SnO_2 and the spiro-OMeTAD interfaces. Hence, in line with what we discussed so far, the spiro-OMeTAD might be the limiting interface.

The work by Abate *et al.*[37] explored the role of dopants, including oxygen due to air exposure and voluntary insertion of Li-TFSI, on the V_{OC} of solid-state, spiro-OMeTAD-based dye-sensitized solar cells. There, it was found that increasing the concentration of Li-TFSI leads to a decrease in the V_{OC}. The effect of oxygen-free conditions on the V_{OC} of state-of-the-art devices with high V_{OC}'s and efficiencies above 20% was studied to understand the effect of oxygen doping/dedoping on the V_{OC}. Oxygen has been widely studied as a dopant in organic electronics, and therefore it is important to understand its role in the PSC performance.[37,38] PTAA PSCs with 1.183 V in air showed a slight increase to 1.193 V upon exposure to N_2 for only 15 min and showed no further increase after additional hundreds of minutes as shown in Fig. 4b. Given that PTAA devices consistently exhibit relatively low V_{OC}'s, it is very likely that the oxygen dedoping effect, which affects trap states,[38] is

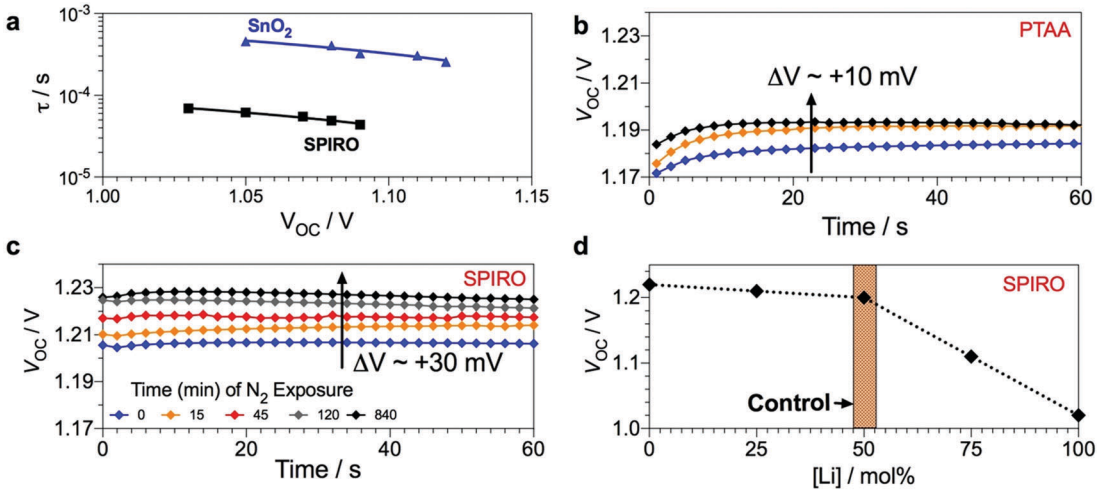

Fig. 4 Perovskite solar cell interfaces limiting V_{OC}. (a) IMVS measurements presenting the recombination constant as a function of V_{OC} (light intensity) for a device as measured from the SnO_2 and spiro sides, (b) V_{OC} *vs.* time with nitrogen exposure for top-performing devices using PTAA and (c) spiro-OMeTAD as HSLs. Devices are kept in nitrogen in the dark and measured after a defined time under 1 sun illumination. (d) V_{OC} *vs.* Li-TFSI dopant concentration for spiro-OMeTAD, measured in air.

masked by the already disordered nature of this HSL. Therefore, the effect of oxygen dedoping on the V_{OC} is negligible.

On the other hand, the effect of oxygen dedoping on high performance spiro-PSCs is remarkable. Fig. 4c shows a device furnishing 1.2 V before nitrogen exposure and up to 1.23 V after 840 min of N_2 exposure. To further understand the effect of dopants, we modified the concentration of Li-TFSI in spiro-OMeTAD and measured the respective V_{OC} in air, as shown in Fig. 4d. Remarkably, the V_{OC} of undoped devices reached a value of 1.22 V, and this value decreased as the concentration of Li-TFSI was increased. Devices containing 25% Li-doping (or 1 : 4 mol : mol) yielded 1.21 V, whereas high-performance devices (''Control'', 50% doping) with an optimized trade-off between V_{OC} and FF yielded 1.20 V. Increasing the concentration further led to poorer performance, where 75% and 100% (1 : 1 molar ratio) doping yielded 1.11 and 1.02 V, respectively. This demonstrates that doping concentration, be it *via* Li addition or environmental oxygen, dramatically affects the recombination dynamics in the device and therefore is a significant factor affecting the V_{OC} of PSCs with state-of-the-art perovskite films. Therefore, dopants act as recombination centers at the HSL interface and dominate recombination dynamics over *e.g.* the energetics of the HTM which is secondary as shown in a recent study by Belisle *et al.*[39]

On the other hand, when aiming for V_{OC} larger than 1.25 V, further optimization of the perovskite film and the overall device architecture are also expected to be required.

Conclusion

We investigated open-circuit voltage changes due to recombination at the interfaces of PSCs, including the charge selective contacts and the effect of grain boundaries. We found that the density of grain boundaries in a highly efficient PSC does not modify the recombination dynamics at 1 sun illumination, for grains larger than 100 nm. Instead, the recombination is strongly dominated by the dopants in the hole transporting material, spiro-OMeTAD and PTAA. The reduction of doping concentrations for spiro-OMeTAD yielded V_{OC}'s as high as 1.23 V; a significant boost from 1.2 V. This work reveals the important role that dopants play in recombination dynamics in PSCs and suggests that better hole transport materials with more selective properties need to be developed, in particular regarding the choice and concentration of additives.

Acknowledgements

M. G. and W. T. thank the King Abdulaziz City for Science and Technology (KACST) for financial support under a joint research project. E. H. A. acknowledges the Ministry of Science, Research and Technology of Iran and Iran Nanotechnology Initiative Council for the financial support. M. S. acknowledges the support from the co-funded Marie Skłodowska Curie fellowship, H2020 Grant agreement no. 665667. Financial support is acknowledged from the Swiss National Science Foundation (SNSF), funding from the framework of the Umbrella project (Grant Agreement no. 407040-153952 and 407040-153990); the NRP 70 ''Energy Turnaround''; in the 9th call proposal 906: CONNECT PV as well as from SNF-NanoTera and Swiss Federal Office of Energy (SYNERGY).

References

1 A. Kojima, K. Teshima, Y. Shirai and T. Miyasaka, *J. Am. Chem. Soc.*, 2009, **131**, 6050–6051.
2 National Renewable Energy Laboratory, Best Research-Cell Efficiencies chart, www.nrel.gov/ncpv/images/efficiency_chart.jpg, accessed July 30, 2016.

3 J.-P. Correa-Baena, A. Abate, M. Saliba, W. Tress, T. Jesper Jacobsson, M. Gratzel and A. Hagfeldt, *Energy Environ. Sci.*, 2017, **10**, 710–727.
4 N. Pellet, P. Gao, G. Gregori, T. Y. Yang, M. K. Nazeeruddin, J. Maier and M. Grätzel, *Angew. Chem., Int. Ed.*, 2014, **53**, 3151–3157.
5 C. C. Stoumpos, C. D. Malliakas and M. G. Kanatzidis, *Inorg. Chem.*, 2013, **52**, 9019–9038.
6 R. E. Brandt, V. Stevanović, D. S. Ginley and T. Buonassisi, *MRS Commun.*, 2015, **5**, 265–275.
7 G. Xing, N. Mathews, S. Sun, S. S. Lim, Y. M. Lam, M. Grätzel, S. Mhaisalkar and T. C. Sum, *Science*, 2013, **342**, 344–347.
8 S. D. Stranks, G. E. Eperon, G. Grancini, C. Menelaou, M. J. Alcocer, T. Leijtens, L. M. Herz, A. Petrozza and H. J. Snaith, *Science*, 2013, **342**, 341–344.
9 W. Tress, N. Marinova, O. Inganäs, M. K. Nazeeruddin, S. M. Zakeeruddin and M. Graetzel, *Adv. Energy Mater.*, 2015, **5**, 1400812.
10 W. Tress, *Adv. Energy Mater.*, 2017, 1602358.
11 J. Gong, S. B. Darling and F. You, *Energy Environ. Sci.*, 2015, **8**, 1953–1968.
12 E. H. Anaraki, A. Kermanpur, L. Steier, K. Domanski, T. Matsui, W. Tress, M. Saliba, A. Abate, M. Gratzel, A. Hagfeldt and J.-P. Correa-Baena, *Energy Environ. Sci.*, 2016, **9**, 3128–3134.
13 W. S. Yang, J. H. Noh, N. J. Jeon, Y. C. Kim, S. Ryu, J. Seo and S. I. Seok, *Science*, 2015, **348**, 1234–1237.
14 M. Saliba, S. Orlandi, T. Matsui, S. Aghazada, M. Cavazzini, J.-P. Correa-Baena, P. Gao, R. Scopelliti, E. Mosconi, K.-H. Dahmen, F. De Angelis, A. Abate, A. Hagfeldt, G. Pozzi, M. Graetzel and M. K. Nazeeruddin, *Nat. Energy*, 2016, **1**, 15017.
15 D. Bi, W. Tress, M. I. Dar, P. Gao, J. Luo, C. m. Renevier, K. Schenk, A. Abate, F. Giordano, J. P. Correa Baena, J.-D. Decoppet, S. M. Zakeeruddin, M. K. Nazeeruddin, M. Grätzel and A. Hagfeldt, *Sci. Adv.*, 2016, **2**, e1501170.
16 M. Saliba, T. Matsui, K. Domanski, J.-Y. Seo, A. Ummadisingu, S. M. Zakeeruddin, J.-P. Correa-Baena, W. R. Tress, A. Abate, A. Hagfeldt and M. Grätzel, *Science*, 2016, **354**, 206–209.
17 M. Saliba, T. Matsui, J.-Y. Seo, K. Domanski, J.-P. Correa-Baena, M. K. Nazeeruddin, S. M. Zakeeruddin, W. Tress, A. Abate, A. Hagfeldt and M. Gratzel, *Energy Environ. Sci.*, 2016, **9**, 1989–1997.
18 J. P. Correa Baena, L. Steier, W. Tress, M. Saliba, S. Neutzner, T. Matsui, F. Giordano, T. J. Jacobsson, A. R. Srimath Kandada, S. M. Zakeeruddin, A. Petrozza, A. Abate, M. K. Nazeeruddin, M. Gratzel and A. Hagfeldt, *Energy Environ. Sci.*, 2015, **8**, 2928–2934.
19 T. J. Jacobsson, J.-P. Correa-Baena, E. Halvani Anaraki, B. Philippe, S. D. Stranks, M. E. F. Bouduban, W. Tress, K. Schenk, J. Teuscher, J.-E. Moser, H. Rensmo and A. Hagfeldt, *J. Am. Chem. Soc.*, 2016, **138**, 10331–10343.
20 J. M. Ball, S. D. Stranks, M. T. Horantner, S. Huttner, W. Zhang, E. J. W. Crossland, I. Ramirez, M. Riede, M. B. Johnston, R. H. Friend and H. J. Snaith, *Energy Environ. Sci.*, 2015, **8**, 602–609.
21 J.-P. Correa-Baena, M. Anaya, G. Lozano, W. Tress, K. Domanski, M. Saliba, T. Matsui, T. J. Jacobsson, M. E. Calvo, A. Abate, M. Grätzel, H. Míguez and A. Hagfeldt, *Adv. Mater.*, 2016, **28**, 5031–5037.
22 R. Marschall, *Adv. Funct. Mater.*, 2014, **24**, 2421–2440.
23 T. G. Allen and A. Cuevas, *Appl. Phys. Lett.*, 2014, **105**, 031601.
24 W. Tress, J. P. Correa Baena, M. Saliba, A. Abate and M. Graetzel, *Adv. Energy Mater.*, 2016, **6**, 1600396.
25 C. G. Bischak, E. M. Sanehira, J. T. Precht, J. M. Luther and N. S. Ginsberg, *Nano Lett.*, 2015, **15**, 4799–4807.
26 H. D. Kim, H. Ohkita, H. Benten and S. Ito, *Adv. Mater.*, 2016, **28**, 917–922.
27 D. W. de Quilettes, S. M. Vorpahl, S. D. Stranks, H. Nagaoka, G. E. Eperon, M. E. Ziffer, H. J. Snaith and D. S. Ginger, *Science*, 2015, **348**, 683–686.
28 H.-S. Kim and N.-G. Park, *J. Phys. Chem. Lett.*, 2014, **5**, 2927–2934.
29 J.-H. Im, I.-H. Jang, N. Pellet, M. Grätzel and N.-G. Park, *Nat. Nano*, 2014, **9**, 927–932.
30 J. S. Yun, A. Ho-Baillie, S. Huang, S. H. Woo, Y. Heo, J. Seidel, F. Huang, Y.-B. Cheng and M. A. Green, *J. Phys. Chem. Lett.*, 2015, **6**, 875–880.
31 X. Ren, Z. Yang, D. Yang, X. Zhang, D. Cui, Y. Liu, Q. Wei, H. Fan and S. Liu, *Nanoscale*, 2016, **8**, 3816–3822.
32 J.-Y. Seo, T. Matsui, J. Luo, J.-P. Correa-Baena, F. Giordano, M. Saliba, K. Schenk, A. Ummadisingu, K. Domanski, M. Hadadian, A. Hagfeldt, S. M. Zakeeruddin, U. Steiner, M. Grätzel and A. Abate, *Adv. Energy Mater.*, 2016, **6**, 1600767.
33 N. Marinova, W. Tress, R. Humphry-Baker, M. I. Dar, V. Bojinov, S. M. Zakeeruddin, M. K. Nazeeruddin and M. Grätzel, *ACS Nano*, 2015, **9**, 4200–4209.
34 V. D'Innocenzo, A. R. Srimath Kandada, M. De Bastiani, M. Gandini and A. Petrozza, *J. Am. Chem. Soc.*, 2014, **136**, 17730–17733.
35 A. Pockett, G. E. Eperon, T. Peltola, H. J. Snaith, A. Walker, L. M. Peter and P. J. Cameron, *J. Phys. Chem. C*, 2015, **119**, 3456–3465.
36 E. Guillén, F. J. Ramos, J. A. Anta and S. Ahmad, *J. Phys. Chem. C*, 2014, **118**, 22913–22922.
37 A. Abate, T. Leijtens, S. Pathak, J. Teuscher, R. Avolio, M. E. Errico, J. Kirkpatrik, J. M. Ball, P. Docampo, I. McPherson and H. J. Snaith, *Phys. Chem. Chem. Phys.*, 2013, **15**, 2572–2579.
38 J. Schafferhans, A. Baumann, A. Wagenpfahl, C. Deibel and V. Dyakonov, *Org. Electron.*, 2010, **11**, 1693–1700.
39 R. A. Belisle, P. Jain, R. Prasanna, T. Leijtens and M. D. McGehee, *ACS Energy Lett.*, 2016, **1**, 556–560.

